Mon. Not. R. Astron. Soc. **000**, 000–000 (0000) Printed 19 September 2006 (MN LATEX style file v2.2)

The spherical collapse model with shell crossing

M.A. Sánchez-Conde[1⋆], J. Betancort-Rijo[2,3] & F. Prada[1],
[1] *Instituto de Astrofisica de Andalucia (CSIC), E-18008, Granada, Spain*
[2] *Instituto de Astrofisica de Canarias, C/ Via Lactea s/n, Tenerife, E38200, Spain*
[3] *Facultad de Fisica, Universidad de La Laguna, Astrofisico Francisco Sanchez, s/n, La Laguna Tenerife, E38200, Spain*

19 September 2006

ABSTRACT
In this work, we study the formation and evolution of dark matter halos by means of the spherical infall model with shell-crossing. We present a framework to tackle this effect properly, that does not involve the adiabatic approximation, and is based on the numerical follow-up, with time, of that individual shell of matter that contains always the same fraction of mass with respect to the total mass. In this first step, we do not include angular momentum, velocity dispersion or triaxiality. Within this framework - named as the Spherical Shell Tracker (SST) - we investigate the dependence of the evolution of the halo with virial mass, with the adopted mass fraction of the shell, and for different cosmologies. We find that our results are very sensitive to a variation of the halo virial mass or the mass fraction of the shell that we consider. However, we obtain a negligible dependence on cosmology. Furthermore, we show that the effect of shell-crossing plays a crucial role in the way that the halo reaches the stabilization in radius and the virial equilibrium. We find that the values currently adopted in the literature for the actual density contrast at the moment of virialization, δ_{vir}, may not be accurate enough. In this context, we stress the problems related to the definition of a virial mass and a virial radius for the halo.

Key words: cosmology:theory — dark matter — large-scale structure of universe — methods:numerical

1 INTRODUCTION

In the hierarchical scenario for structure formation in the Universe, the small primordial density fluctuations grow due to non-linear gravitational evolution and finally become the first virialized structures (halos). In this picture, larger Cold Dark Matter (CDM) halos will be formed by the accretion and merger of those first smaller halos, forming in this way massive structures, and so on. This scenario, that constitutes the actual paradigm of hierarchical structure formation, is able to explain in general terms the universe that we see today. Yet, we do not have a framework or theory capable of reproducing this picture accurately. In this context, N-body cosmological simulations are a powerful tool to try to understand the formation and subsequent evolution of CDM halos. They constitute a very important help to build any theoretical model and their predictions explain many of different observations.

Basically, there are two analytical approaches that make the problem tractable, although some simplifications have to be made and, as it was said, comparison between these analytical studies and simulations are crucial to make progress: the Press-Schechter formalism (Press & Schechter 1974), based on the role of mergers (Nusser & Sheth 1999; Manrique et al. 2003), and the spherical infall model (SIM) focused on the understanding of the collapse of individual objects. We must note that in the Press & Schechter formalism, the *SIM* has also been widely used, but from a statistical point of view, to treat problems related to mass accretion histories, mass function, etc. The *SIM*, first developed by Gunn & Gott (1972) and Gunn (1977), describes the collision-less collapse of a spherical perturbation in an expanding background. In those two articles, they introduced for the first time the cosmological expansion and the role of adiabatic invariance in the formation of individual objects. Fillmore & Goldreich (1984) and Bertschinger (1985) found analytical predictions for the density profiles of collapsed objects seeded by scale-free primordial perturbations in a flat universe. Hoffman & Shaham (1985) generalized these solutions to realistic initial profiles in flat and open Friedmann models, and Baarden et al. (1986) (hereafter BBKS) improved this work introducing the peak formalism. Later, some studies have been done to include more realistic dynamics of the growth process of dark matter halos (e.g. Pad-

⋆ E-mail: masc@iaa.es

manabhan 1996; Avila-Reese, Firmani & Hernández 1998; Lokas 2000; Subramanian, Cen & Ostriker 2000).

In parallel, a large amount of numerical work have been done. Quinn, Salmon & Zurek (1986) and Frenk et al. (1988) obtained isothermal density profiles ($\rho \propto r^{-2}$) of CDM haloes, and Dubinski & Carlberg (1991) and Crone, Evrard & Richstone (1994) basically reproduced the predictions of Hoffman & Shaham (1985) and found some evidence for no pure power-law density profiles. Later, it was established that the density profiles of CDM halos have an universal form (Navarro, Frenk & White (1996, 1997, hereafter NFW), with $\rho \propto r^{-1}$ in the inner regions and $\rho \propto r^{-3}$ in the outskirts, although there is still controversy about the shape of the profile near the center and recently it has been found that the profiles flatten out close to $\rho \propto r^{-2}$ beyond ~ 2 virial radius. Moore et al. (1998,1999), amongst others, find $\rho \propto r^{-1.5}$ in the very center and other authors (Jing & Suto 2000; Klypin et al. 2001; Ricotti 2003) find an inner slope ranging from -1 to -1.5 depending on halo mass, merger history and substructure. Concerning to the outskirts of dark matter halos, Prada et al. (2006) carried out a detailed study and concluded that a 3D Sérsic three parameter approximation provides excellent density fits up to ~ 2 times the virial radius, although these profiles differ considerably from the NFW ones beyond 2 virial radius.

There are also plenty of works in the literature using the *SIM* to predict the density profiles of dark matter halos mainly focused on explaining their central regions. Moreover, the *SIM* has been widely used to obtain some quantities specially relevant and directly related to crucial stages in the formation and evolution of CDM haloes for different cosmologies, redshifts, etc. A particularly relevant quantity is the value of the overdensity at the moment of virialization δ_{vir} (Δ_{vir} usually in the literature), where overdensity is defined here as a number of times the background density, and its linear counterpart $\delta_{l,vir}$. The values of $\delta_{l,vir}$ and δ_{vir} were obtained introducing the virial theorem into the *SIM* formalism. This has important implications in the way we define the virial radius (the radius that attains an overdensity δ_{vir} inside) of dark matter halos in N-body cosmological simulations. δ_{vir} is conventionally chosen to be near 180 for an Einstein-deSitter cosmology (e.g. Peebles 1980), or 340 for the $\Omega_\Lambda = 0.7$ cosmology (e.g. Bryan & Norman 1998; Lokas & Hoffman 2000).

In the standard derivation of $\delta_{l,vir}$ and δ_{vir}, the typical way to proceed is to assume that a shell of matter stabilizes at an epoch twice the time of turn-around (i.e. the time predicted by the standard *SIM* to collapse into a point), and in average with a radius that is 1/2 the turn-around radius (e.g. Peebles 1980; Lacey & Cole 1994; Eke, Cole & Frenk 1996). This 1/2 factor (in the Einstein-deSitter cosmology; for other cosmologies we need to use the Lahav equation, Lahav et al. 1991) is called the *collapse factor*. However, the justification to introduce this collapse factor and to suppose the time of virialization as twice the time of turn-around, is poor and lack a solid theoretical background. In contrast, in this work we will study the spherical collapse without supposing any collapse factor, only taking into account the shell-crossing as the dominant effect. The angular momentum and velocity dispersion may also play an important role. The question is: if these effects were included in the model, would we obtain the same values for δ_{vir} and $\delta_{l,vir}$ that those found in the most simplistic scenario described by the standard *SIM*? This issue is one of the aims of the present work.

The main goal of this line of work is to develop a theoretical framework that help us to understand the dynamical elements that determine the process of formation of structures (collapsed objects) using spherical symmetry to explain main properties of dark matter halos. In this first work we will tackle these questions by means of a "cold" collapse, that is, without including the effects of the velocity dispersion and angular momentum. The point is to ascertain if the non-uniformity of the density profiles generated via shell-crossing is able to provide the radial motions necessary to produce the virialization and stabilization in an appropriate time scale. In a future work, we will include the angular momentum and velocity dispersion to go a step further.

There are some issues that it is worth to mention and that make this work different from previous works that also included the shell-crossing in their formalism (e.g. Lokas & Hoffman 2000; Nusser 2001; Hiotelis 2002; Ascasibar et al. 2004). The way to proceed in these works is to handle the effect of shell-crossing by means of an adiabatic invariant, once the standard *SIM* becomes incorrect for late stages of the evolution. This adiabatic invariant, also known as *radial action*, makes the problem analytically tractable, and is based on the fact that the potential evolves in a time larger than the orbital period of the most inner shells. In contrast, we will study the shell-crossing effect doing a follow-up of the radius that contains inside always the same fraction of the virial mass. This way to tackle the problem is only one of the possible options, but is essential, for example, in order to build and study the relationship between the actual enclosed density contrast δ, defined as $\delta = \frac{\rho(<r) - <\rho_m>}{<\rho_m>}$, with $<\rho_m>$ the mean matter density of the Universe, and the linear density contrast, δ_l, obtained from the linear theory. Only Gehard Lemson did something similar, although using N-body simulations and mainly focused on showing how accurate are the predictions of the standard *SIM* compared to his simulations (Lemson 1995). Despite the fact that he showed that the *SIM* is a powerful tool to understand the evolution of halos, he never provided detailed quantities and relations for the actual and linear density contrasts. The function $\delta_l(\delta)$ is very important to obtain the density profiles of dark matter halos, as we discussed in previous works (Prada et al. 2006; Betancort-Rijo et al. 2006). Sheth & Tormen (2002) parametrized this function for the standard *SIM*. The framework presented here will allow us in the near future to provide also a simple parametrization for $\delta_l(\delta)$, but taking into account the important effect of shell-crossing, together with others relevant effects such as the angular momentum and velocity dispersion. This will lead us, for example, to obtain $\delta_{l,vir}$ and its corresponding δ_{vir}, to explain the shape of the dark matter density profiles or to shed light on the mass functions. All of this without supposing any collapse factor, as pointed before, or other vague assumptions. Nevertheless, it will not be possible to obtain useful applications for the moment, since in this first work we will include in our study only the shell-crossing, which is the dominant effect. The full treatment will be done and presented in an upcoming work. Here we will provide the first results of our theoretical framework related to the role played by the shell-crossing.

The paper is organized as follows. In section 2 we briefly describe the *SIM* and explain the formalism and unities that we will use in the rest of the work. In section 3 we will study in detail the dependence of the way that the evolution occurs varying some parameters, in particular, the virial mass of the halo, the fraction of mass for a given virial mass, and the cosmology. Section 4 will be specially dedicated to the moments of virialization and stabilization according to a given criterion, and their dependence with the same parameters described above. We will also emphasize here the difference between these two concepts. Finally, in section 5, we address the main results and ideas of the work, and point the lines for a future work.

2 THE SPHERICAL SHELL TRACKER FRAMEWORK

In this section, we first describe the standard *SIM* and its equations, and then we present the formalism that we will use in the rest of the work, which will imply to describe the density profile and define our own unities. This will allow us to handle easily the equations involved. Later, the algorithm that we used to obtain the results will be described carefully step by step. All together will be known as the Spherical Shell Tracker Framework (*SST*). The main objective of this section is to make easier a possible reproduction and implementation of the *SST* framework.

2.1 The formalism

In a flat Universe with $\Omega_\Lambda = 0$, the evolution of a homogeneous spherical (positive) density perturbation (the simplest way to tackle the problem of structure formation) with a mass M and radius R, is given by Newtonian dynamics (as shown by Tolman 1934 and Bondi 1947), provided that R be much smaller than the Hubble radius:

$$\frac{d^2R}{dt^2} = \frac{-G\ M}{R^2} \tag{1}$$

Integrating, since M is constant by definition, we obtain:

$$\frac{1}{2}\frac{dR}{dt^2} - \frac{G\ M}{R} = E \tag{2}$$

where E determines whether the sphere expands forever ($E > 0$) or it finally contracts ($E < 0$).

We can describe in more detail this spherical perturbation with a large number of mass particles, and even it is possible and more useful to imagine these particles as concentric shells (thanks to spherical symmetry) that do not cross each other, and each of them with a radius $r(j,t)$, where j denotes the shell, which satisfies equation (1):

$$\frac{d^2r(j,t)}{dt^2} = \frac{-G\ M(j,t)}{r(j,t)^2} \tag{3}$$

where $M(j,t)$ is the enclosed mass for each shell j at time t:

$$M(j,t) = \rho_{crit}\left(\frac{4\pi}{3}r(j,t)^3\right)[1+\delta(r(j,t))] \tag{4}$$

being ρ_{crit} the critical density of the Universe, and $\delta(r)$ the actual density contrast within $r(j,t)$:

$$\rho_{crit} = \frac{3\ H^2}{8\pi\ G}; \qquad \delta(r) = \frac{\rho(<r) - <\rho_m>}{<\rho_m>} \tag{5}$$

with H the Hubble constant, and $<\rho_m>$ the mean matter density of the Universe.

As long as shell-crossing does not occurs, the actual density contrast is related to the linear one (given by the linear theory, see e.g. Padmanabhan 1993) in the Einstein-deSitter cosmology by the formula (Sheth & Tormen 2002):

$$\delta_l(\delta) = \left[1.68647 - \frac{1.35}{(1+\delta)^{2/3}} - \frac{1.12431}{(1+\delta)^{1/2}} + \frac{0.78785}{(1+\delta)^{0.58661}}\right] \tag{6}$$

The inverse function, $\delta(\delta_l)$, is given by (Patiri et al. 2004):

$$\delta(\delta_l) = 0.993\Big[(1 - 0.607(\delta_l - 6.5\times10^{-3}(1-\theta(\delta_l)+$$
$$+\theta(\delta_l - 1.55))\delta_l^2))^{-1.66} - 1\Big] \tag{7}$$

being θ the step function:

$$\theta(x) = \begin{cases} 1 & \text{if x} > 0 \\ 0 & \text{if x} \leqslant 0 \end{cases}$$

It is possible to make some simplifications in the equations, choosing in an appropriate manner the value of some parameters. In particular, we choose:

$$\text{time unit} = \text{initial time}$$
$$\text{length unit} = \text{initial radius of the protohalo, } R_i$$
$$\text{mass unit} = [1+\delta(R_i)]$$

According to these units, and taking into account equations (4) and (5), and an Einstein-deSitter cosmology (where $H = \frac{2}{3}t^{-1}$), we have:

$$H_i = \frac{2}{3}; \qquad \rho_{crit,i} = \frac{3}{4\pi}; \qquad G = \frac{2}{9} \tag{8}$$

where i refers to the initial time.

The Lagrangian radius q for each shell j (i.e. the comoving radius at $t \to 0$) is related to the Eulerian one r by:

$$q(j) = r_i(j)\ [1+\delta(r_i(j))]^{\frac{1}{3}} \tag{9}$$

So, for the initial enclosed mass of a shell j, we now have simply (in our units and using Eq.(4)):

$$M(j,t_i) = M(j) = q(j)^3 \tag{10}$$

We must note that this enclosed mass of a shell j, $M(j)$, is different from the mass of each shell, $M_{shell}(j)$:

$$M_{shell}(j) = M(j) - M(j-1)$$

$$M(j,t) = \sum_{i=1}^{n} M_{shell}(i) \qquad \text{always than } r(i) \leqslant r(j) \tag{11}$$

To obtain $q(j)$ using Eq.(9) we need $\delta^i(r_i(j))$, that is, the actual density contrast at initial time, and to this end we need the linear profile at initial time, $\delta_l^i(q(j))$. In this work we will use the linear profile presented in Prada et al. (2006) and Betancort-Rijo et al. (2006):

$$\delta_l(q) = \delta_{l,vir}\frac{\sigma_{12}(q)}{\sigma(Q)} \tag{12}$$

Table 1. Values of b and Q necessary to use the approximation for δ_0 given by (14).

M ($h^{-1}M_\odot$)	Q (h^{-1}Mpc)	b
6.5×10^{10}	0.57	0.1889
5×10^{11}	1.1252	0.2202
3×10^{12}	2.0445	0.2544
2×10^{13}	3.848	0.301
5×10^{14}	11.125	0.41

where $\delta_{l,vir}$ is the linear density contrast at the moment of virialization, q and Q are the Lagrangian radii related to r and R_{vir} respectively, that can be obtained using equation (9), and:

$$(\sigma(x))^2 = \frac{1}{2\pi^2} \int_0^\infty \mid \delta_k \mid^2 W_T^2(xk)\ k^2\ dk$$

$$\sigma_{12} = \sigma_{12}(q) = \frac{1}{2\pi^2} \int_0^\infty \mid \delta_k \mid^2 W_T(qk)\ W_T(Qk)\ k^2\ dk$$

$$W_T(x) = \frac{3(sin\ x\ - x\ cos\ x\ )}{x^3} \tag{13}$$

where $|\delta_k|^2$ stands for the power spectra of the density fluctuations linearly extrapolated to the present.

There is a good approximation for δ_0:

$$\delta_l(q) = \delta_{l,vir}\ exp\left[-b\left(\left(\frac{q}{Q}\right)^2 - 1\right)\right]$$

$$b(Q) = -\frac{1}{2}\ \frac{d\ln\sigma(x)}{d\ln x}\bigg|_{x=Q} \tag{14}$$

with b a constant depending on the mass. In Table 1 we present the values of b and Q that we use for each mass. Moreover, it is necessary to assign a value to $\delta_{l,vir}$ so that we can use the density profile, although one of our final goals is to obtain a precise value for it. In this work we used a $\delta_{l,vir} = 1.9$, a value which led to good results in previous works (Prada et al. 2006; Betancort-Rijo et al. 2006).

Essentially, the profile given in Eq.(12) and its approximation in Eq.(14) takes into account only the restriction $\delta_l(Q) = \delta_{l,vir}$. In Hiotelis (2002) and Ascasibar et al. (2004), a very similar density profile was also used, but using the BBKS peak formalism to compute the initial conditions. In a future work we will use a more sophisticated density profile that includes also the restriction $\delta_l(q) < \delta_{l,vir}$ for $q > Q$ (see Betancort-Rijo et al. (2006) for a more detailed description), resulting in steeper actual density profiles for smaller masses (as confirmed by numerical simulations, see Prada et al. 2006). This fact will probably change slightly the results. For the sake of simplicity we have chosen to use now a simple profile, although the major results of this work will not depend on the assumed profile.

For the Einstein-deSitter cosmology, the $\delta_l^i(q(j))$ profile can be obtained from equation (12) simply rescaling by:

$$\delta_l^i(q(j)) = \frac{1}{1+z_i}\ \delta_l(q(j)) \tag{15}$$

where z_i is the redshift at initial time. We can obtain $\delta^i(r_i(j))$ from $\delta_l^i(q(j))$ using the function given in (7). Inserting this $\delta(\delta_l^i(q(j)))$ in Eq.(9) we obtain the Lagrangian radius for each shell j, $q(j)$, and also using Eq.(10 its enclosed mass $M(j)$.

Once we have the expressions related to the initial conditions and we have presented the density profile, we need the equations of evolution. If the shells do not cross each other, then there is an analytical solution for (2) (e.g. Martínez & Saar 2002) that can be written in the parametric form:

$$r = r_c(1 - cos\eta); \quad t = t_c(\eta - sin\eta) \tag{16}$$

where:

$$r_c = \frac{GM}{c^2}; \quad t_c = \frac{r_c}{c}; \qquad \frac{dt}{d\eta} = \frac{R}{c} \tag{17}$$

Here c is the velocity of light and we did a change to a non-dimensional variable η. This solution means that the shell expands until it reaches a maximum radius r_{ta}, the turn-around radius, at a given time t_{ta}, which is different for each shell, and after that point the shell starts to contract. We can integrate analytically equation (3) to study the evolution of the spherical density perturbation, at least until the turn-around, thanks to the fact that the enclosed mass of the shells do not change with time. Nevertheless, after the turn-around, the re-collapse begins and the shell-crossing also starts, so we can not proceed in the same way. At that point, it is common to use a prescription based on an adiabatic invariant, to account for this secondary infall and shell-crossing (e.g. Lokas & Hoffman 2000; Nusser 2001; Hiotelis 2002; Ascasibar et al. 2004). On the other hand, one can also integrate numerically the equation (3), computing at each time step the new radius, velocity and enclosed mass for each shell. This is the method that we use in our work. Our purpose is to study and to include the shell-crossing in our treatment in a natural way, i.e. without making any assumption about the collapse factor, the time at which virialization occurs, or any other simplification.

We first divide our spherical density perturbation in n equal spherical shells (equivalent to particles), all of them with the same thickness, and later we choose the shell j that contain a given fraction of mass of the total protohalo. We do so for every time step, from the start of the evolution to the end: we recompute the new enclosed mass for each shell at each time step, and we always select that one that contains the fraction of mass we are interested in (in that sense, n must be big enough to choose with high precision and without problems at each step a shell that contains exactly the required fraction of mass; in our case, $n = 3000$ was enough). If we follow for a long time the shell related to this fraction of mass, at the end its radius will be almost constant (although the corresponding physical shell will change with time), that is, we will reach stabilization (see section 4). Lu et al. (2006) used a similar algorithm, but they divided the halo in equal mass shells, instead of shells with the same thickness, as we do. Moreover, their motivations were different, mainly focused on explain the inner shape of the density profiles, and they did not carried out a follow-up of any shell in particular.

2.2 The algorithm

We now describe the algorithm we used to compute the relevant quantities (radius, velocity and enclosed mass) for each shell at each time step.

First, we need to obtain the *initial conditions*:

(i) We divide the protohalo in n equal shells to calculate our array of initial radii, $r_i(j)$, that contains the radius r for all the shells. Remember that, in our units, the radius of the total cloud is unity; moreover, j increases decreasing the radius, so $r(j=1) = R_i$ (the radius of the whole halo), and $r(j=3000)$ is the radius of the deepest shell.

(ii) In a first approximation, we make $q(j) = r_i(j)$. This will allow us to compute a second and better estimation for $q(j)$ using in an appropriate way the relation given by equation (9), that is:

$$q(j) = r_i(j)[1+\delta(\delta_l^i(q(j)))]^{\frac{1}{3}} \tag{18}$$

where we introduce in the right side the $q(j)$ as given by the first approximation. The function $\delta(\delta_l)$ is given by eq.(7) and $\delta_l^i(q(j))$ is given by (15).

(iii) Now, we will use the $q(j)$ obtained in the last step as a new approximation to compute again a better estimation for $q(j)$, according to eq.(18).

(iv) Step (iii) must be repeated until there is no difference between the $q(j)$ that we obtain after each iteration, or this difference is less than at least 5% between two consecutive iterations.

(v) With $r_i(j)$ and the last and best estimations for the initial Lagrangian radii of the shells, $q(j)$, we can calculate the initial enclosed mass array, $M(j)$, using equation (10), and the mass of each shell, $M_{shell}(j)$, knowing that $M_{shell}(j) = M(j) - M(j-1)$. We will need $M_{shell}(j)$ later to compute the enclosed mass array at each time step, since the mass of each shell will be always the same, although the order of the shells will be modified.

(vi) We also need the initial velocity for each shell, $v_i(j)$, as given by the *SIM* (Betancort-Rijo et al. 2006):

$$v_i(j) = H_i\ r_i(j)\ \left[1 - \frac{1}{3}\frac{1}{1+\delta(\delta_l^i(q(j)))} \times \frac{1}{\frac{d\delta_l(\delta)}{d\delta}|_{\delta=\delta(\delta_l^i(q(j)))}}\ \delta_l^i(q(j))\right] \tag{19}$$

where $\delta_l(\delta)$ and $\delta(\delta_l)$ are given by Eq.(6) and Eq.(7), and $\delta_l^i(q(j))$ is given by Eq.(15). H_i is the Hubble constant at initial time, which in our units is $H_i = 2/3$.

(vii) Now it is possible to select the shell that contains the fraction of mass that we are interested in. Our studies will be focused on the follow-up of this shell in particular.

Once we have calculated the initial conditions, we now need to obtain the *equations of evolution*:

(viii) In our units, equation (3) can be written as:

$$\frac{d^2r(j,t)}{dt^2} = -\frac{2}{9}\frac{M(j,t)}{r(j,t)^2} \tag{20}$$

so the equations of the evolution for $r(j)$ and $v(j)$ are:

$$r(j,t+\Delta t) = r(j,t) + v(j,t)\ \Delta t \tag{21}$$

$$v(j,t+\Delta t) = v(j,t) - \frac{2}{9}\frac{M(j,t)\ \Delta t}{r(j,t)^2} \tag{22}$$

(ix) We also need to compute how the linear and actual density contrasts evolve with time:

$$\delta_l(j,t) = \delta_l^i(q(j))\ t^{\frac{2}{3}} \tag{23}$$

$$\delta(j,t) = \left[[1+\delta(\delta_l^i(q(j)))]\left(\frac{r_i(j)}{r(j)}\right)^3\right] t^2 - 1 \tag{24}$$

(x) At each time step, we need to recalculate the new enclosed mass array, $M(j)$, using the shell mass array $M_{shell}(j)$, since the enclosed mass for a given shell j is equal to:

$$M(j,t) = \sum_{i=1}^{n} M_{shell}(i) \qquad \text{always than } r(i) \leqslant r(j) \tag{25}$$

(xi) At this point, we can select again the shell that contains that fraction of mass we want to study, to see what happens with its radius, velocity, and linear and actual density contrasts.

(xii) For each step, we will have to repeat (ix) to (xii).

It is worth to mention, for possible reproductions of the results, that the beginning was set to an initial redshift $z_i = 15$, to make sure that we are still well inside the linear regime, i.e. the initial value of δ_l is small enough. Moreover, we used an optimized temporal step of 0.003 in our units, which is good enough to give us robust results of δ_l and δ (we checked these values using well known moments of the evolution like the turn around, where there is no shell-crossing yet).

Furthermore, there is another important question that it is necessary to take into account to implement without problems the described algorithm. This is the fact that we have not included yet the effect of the velocity dispersion and angular momentum. Therefore, we are in a totally radial (*cold*) collapse and we will have problems in the very center of the halo if we simply integrate numerically the equations following this framework. When we compute, according to equations (21) and (22), the new radius and velocity of a shell which is located very near to the center, we can obtain at the following time step a negative radius and a positive velocity, which means that actually this shell has crossed through the center and now it goes from the inner regions of the halo to the outer ones. In these circumstances, energy is not exactly conserved due to numerical reasons. The distance that the shell covers in only one time step is comparable to its radius, which gives a considerable "leak" of energy. There are different ways to solve this problem; one of them, the solution we chose, is to define a parameter m to measure properly this effect and to help us to prevent this lost of energy. If we define for each shell the parameter m as $m = \Delta r/r(j,t)$ (where $\Delta r = r(j,t+\Delta t) - r(j,t)$ is the distance that the shell has covered along this time step), then there is no problem while m is small enough, but when m reaches a larger value, the way to minimize the lost of energy in the process is to change the velocity by its absolute value, and keeping intact the value that we have for the radius. Doing so, we *skip* the very center and the loss of energy will be minimum. After many attempts, we saw that a value of $m = 0.02$ leads to very good results. Once ve-

locity dispersion and angular momentum are included, this parameter m will not be necessary.

In the ΛCDM cosmology, the formalism and the algorithm are the same, but we must introduce some changes in the initial conditions and in the equations of the evolution the spherical to take into account the different cosmology with $\Lambda \neq 0$. The equations, modified adequately, are presented in Appendix A.

3 THE EVOLUTION OF THE HALO: EFFECT OF SHELL-CROSSING

At the beginning of the evolution, we will not obtain any difference using our formalism or using the standard *SIM*, because there is no shell-crossing yet. However, when this effect starts it is clear that this will become false. However, the expected deviation with respect to that given by the standard *SIM* may be different if one uses different values for the virial mass of the halo, or study different fractions of mass with respect to this virial mass, or if we move to a different cosmology. To this end, that is, to quantify in detail how big are the dependences on these factors, we carried out a study varying the virial mass of the halo, M_{vir}, the fraction of mass related to this virial mass, that we call M_{frac}, and the cosmology through the value of Ω_Λ.

To illustrate the way in which shell-crossing occurs and affects to the evolution of the halo, in Figure 1 we show the evolution with time of the radius related to different M_{frac} for the particular case of an Einstein-deSitter cosmology and a virial mass of $M_{vir} = 3\times10^{12}h^{-1}M_\odot$. Both the radius and time are expressed in units of the turnaround values (so we can compare between different M_{frac} in the same scale). It is worth to mention that Lemson (1995) presented in the same way data from his simulations and he obtained essentially the same results as shown here for the evolution of individual shells.

Before the first shell-crossing happens, the behaviour of the radii of different M_{frac} is essentially the same. This first shell-crossing occurs just before twice the time of turnaround (the time of virialization for the usual models), and what we can see is that this first shell-crossing means the beginning of the stabilization in radius, which finally occurs some time after that (in next section, we will carry out a detailed study of this process together with the virialization). The larger radius oscillations for each curve beyond $\sim 4\ t/t_a$ (see Figure 1) are only noise due to the growth of numerical errors with time, although in the case of $M_{frac} = 1$ the larger deviations at larger times are partially and probably due to border effects, i.e. the shell that contains the required fraction of mass is near the border of the halo at that time, so there are no enough shells above to obtain a good behaviour using our algorithm.

In Table 2 we summarize the results for the linear and actual density contrasts for a halo with virial mass $M_{vir} = 3\times10^{12}h^{-1}M_\odot$ and four values of M_{frac} for two different cosmologies: the Eintein-deSitter and a model with $\Omega_m = 0.3$, $\Omega_\Lambda = 0.7$. In each case, the corresponding values of δ_l and δ are given for critical or interesting moments of the evolution, in particular when the first shell-crossing occurs (FSC), when $\delta = 180$ ($VIR1$), $\delta = 340$ ($VIR2$) and when the collapse occurs (COL) according to the standard *SIM*,

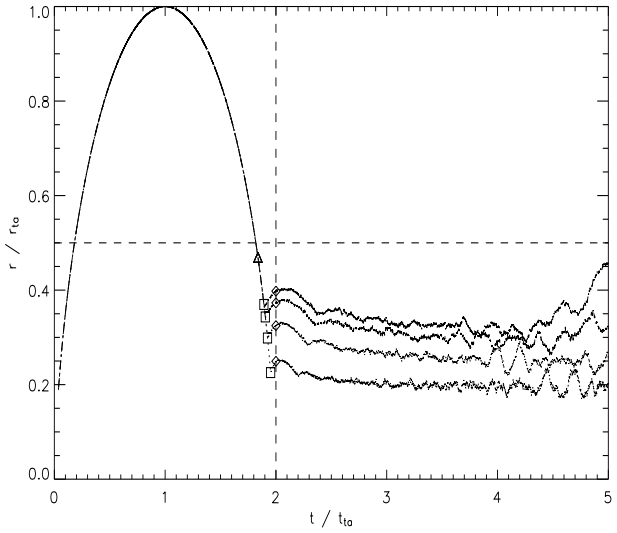

Figure 1. Evolution with time of the radius for different M_{frac}, for a halo with a virial mass $M_{vir} = 3\times10^{12}h^{-1}M_\odot$ and an Einstein-deSitter cosmology. Both radius and time are in units of the turnaround radius and time respectively. From down to top, the curves are for $M_{frac} = 0.2;\ 0.5;\ 0.8;\ 1.0$. Triangle means $\delta = 180$, squares the first shell-crossing, and circles indicate the time of collapse according to the standard *SIM*. The horizontal dashed-line corresponds to half the turnaround radius, and the vertical one the time of collapse, i.e. twice the turnaround time.

that is, twice the time of turn-around. The selection of $VIR1$ and $VIR2$ was done because they are the preferred values of δ_{vir} in the literature for a flat universe with $\Omega_\Lambda = 0$ and $\Omega_\Lambda = 0.7$ respectively. They would be also useful to show a possible dependence (or not) of the function $\delta(\delta_l)$ on the cosmology. It must be noted here that for the $\Omega_\Lambda = 0.7$ cosmology, this value of Ω_Λ is always referred to redshift zero, so the given values of δ_l and δ in this case are actually related to other values of the cosmological constant, i.e. the value of this constant at that time FSC, $VIR1$, $VIR2$ or COL. This fact is common to the rest of tables of the work.

It is important to note here that, although Table 2 is only for a given virial mass, the same kind of study was done for the evolution of halos with virial masses $M_{vir} = 6.5\times10^{10}h^{-1}M_\odot$ and $M_{vir} = 5\times10^{14}h^{-1}M_\odot$. We observed the same tendencies in the data and achieved the same conclusions. In Table 3 we show the values of δ_l and δ that we obtained for the three mentioned virial masses and for the Eintein-deSitter and the $\Omega_m = 0.3$, $\Omega_\Lambda = 0.7$ cosmologies, for the particular case in which we fixed M_{frac}=0.5.

Some interesting conclusions can be inferred from the Figure 1 and Tables 2 and 3. The most important ones can be summarized as follows:

(i) FSC, the first shell-crossing, occurs earlier as M_{frac} increases.

(ii) FSC occurs also earlier for larger masses.

(iii) FSC sets the beginning of the stabilization in radius.

(iv) FSC always occurs after $VIR1$ and $VIR2$ but always before COL, independently of M_{vir} and M_{frac}.

(v) $VIR1$ and $VIR2$ have essentially the same associated linear density contrasts, no matter the value of M_{frac} or

Table 2. Linear (δ_l) and actual (δ) density contrast values related to some important moments in the evolution of a halo with a virial mass $M_{vir} = 3 \times 10^{12} h^{-1} M_\odot$ and for the Einstein-deSitter and $\Omega_m = 0.3$, $\Omega_\Lambda = 0.7$ cosmologies. See text for details, page 6.

Einstein-deSitter ($\Omega_m = 1$, $\Omega_\Lambda = 0$)

	$M_{frac} = 0.2$		$M_{frac} = 0.5$		$M_{frac} = 0.8$		$M_{frac} = 1.0$		$M_{frac} = 1.3$	
Moment	δ_l	δ	δ_l	δ	δ_l	δ	δ_l	δ	δ_l	δ
FSC	1.667	1840	1.652	770	1.641	500	1.634	398	1.628	329
VIR1	1.601	180	1.602	180	1.602	180	1.602	180	1.603	180
VIR2	1.628	340	1.628	340	1.629	340	1.628	340	1.628	340
COL	1.695	1426	1.695	653	1.696	424	1.696	350	1.696	289

$\Omega_m = 0.3$, $\Omega_\Lambda = 0.7$

	$M_{frac} = 0.2$		$M_{frac} = 0.5$		$M_{frac} = 0.8$		$M_{frac} = 1.0$		$M_{frac} = 1.3$	
Moment	δ_l	δ	δ_l	δ	δ_l	δ	δ_l	δ	δ_l	δ
FSC	1.670	1728	1.655	761	1.644	516	1.639	427	1.633	356
VIR1	1.608	180	1.606	180	1.605	180	1.605	180	1.605	180
VIR2	1.632	340	1.632	340	1.631	340	1.631	340	1.631	340
COL	1.698	1364	1.698	338	1.697	445	1.696	380	1.696	320

M_{vir}. This is because in all the cases, there has not been any shell-crossing before $VIR1$ and $VIR2$, so the standard *SIM* is still valid.

(vi) Concerning to the linear and actual density contrasts for a given $M_{frac}$and M_{vir}, there is no substantial difference between the values obtained for different cosmologies.

Specially relevant is the last conclusion, which means that there is no dependence with the cosmology in the values of δ_l and δ, or this dependence is really small and negligible.

Furthermore, we must note here the very high values found for the actual density contrast δ at the moment of the first shell-crossing (FSC) and collapse (COL). The reason for that is that there are other important effects, together with shell-crossing, involved in the formation and evolution of dark matter halos and that we have not included yet in our model. In particular, angular momentum and velocity dispersion will become very relevant and by sure will reduce the values that we obtain for δ. In fact, Avila-Reese, Firmani & Hernández (1998), Hiotelis (2002), Ascasibar et al. (2004) and Shapiro et al. (2004), amongst others, introduce and study the angular momentum and find shallower density profiles in the inner regions, as expected. Hence, it will be absolutely necessary to take into account at least these two effects if we want to go a step further in our analysis and if we want to obtain a good and accurate parametrization for the function $\delta_l(\delta)$. Nevertheless, the framework and algorithm we are using, as well as the conclusions and tendencies we can obtain only including the shell-crossing, are totally valid although we can not reach, by now, exact values. Including other effects in our framework, specially those ones mentioned above, will be part of a future work.

Then, for the moment, we will not be able to provide an exact relation between the linear and actual density contrasts, neither a parametric form for the function $\delta_l(\delta)$. However, we can have a look to the relation that we obtain at this moment between both density contrasts, and try to extract some conclusions. In Figure 2, the function $\delta_l(\delta)$ is represented for the three virial masses under study and for the Einstein-deSitter cosmology. Figure 3 represents the same function but for different cosmologies, in particular for the Einstein-deSitter case and $\Omega_m = 0.3$, $\Omega_\Lambda = 0.7$. The linear region is clearly visible in both figures below $\delta_l \sim 1$. In this regime there is no still any difference between the different curves and the value of δ grows very slowly with δ_l, as expected. Then, there is a phase where δ increases very fast for small differences in δ_l, starting from $\delta_l \sim 1.6$ in all the cases. From this moment, the dependence with virial mass becomes clearly visible in figure 2, where we observe that the smaller the mass, the larger the values of δ attain for the same value of δ_l. Respect to the dependence on different cosmologies, it seems clear (see Figure 3) that this dependence is really small, as already mentioned.

4 STABILIZATION AND VIRIALIZATION

In the standard *SIM* and an Einstein-deSitter cosmology, the value of δ_l corresponding to the final stage of evolution, to the so-called *virialization*, is usually taken as $\delta_{l,vir} = 1.686$, that corresponds to an actual density contrast $\delta_{vir} \approx 180$ (e.g. Peebles 1980). For the $\Omega_m = 0.3$, $\Omega_\Lambda = 0.7$ cosmology, $\delta_{l,vir} = 1.676$ and $\delta_{vir} \approx 340$ (e.g. Lacey & Cole 1994; Eke, Cole & Frenk 1996; Bryan & Norman 1998). As pointed in previous sections, those calculations are based mainly on the following assumptions:

(i) The halo virializes within a radius that is, on average, a given fraction of its maximum radius (the turnaround radius). This fraction is the collapse factor, and is equal to 1/2 in the Einstein-deSitter cosmology, and in other cosmologies it can be inferred from the Lahav equation (Lahav et al. 1991).

(ii) The time at which virialization occurs is twice the time of turn-around, that is, the time at which the collapse happens according to the standard *SIM*.

Although the values inferred for $\delta_{l,vir}$ and δ_{vir} in this way are commonly accepted as the correct ones and are

Table 3. Linear (δ_l) and actual (δ) density contrast values related to some important moments in the evolution of a halo for three different virial masses ($M_{vir} = 6.5 \times 10^{10} h^{-1} M_\odot$, $M_{vir} = 3 \times 10^{12} h^{-1} M_\odot$ and $M_{vir} = 5 \times 10^{14} h^{-1} M_\odot$) and two different cosmologies (Einstein-deSitter and $\Omega_m = 0.3$, $\Omega_\Lambda = 0.7$). A value of $M_{frac} = 0.5$ was set in all the cases. See text for details, page 6.

Einstein-deSitter ($\Omega_m = 1$, $\Omega_\Lambda = 0$)

	$M_{vir} = 6.5 \times 10^{10} h^{-1} M_\odot$		$M_{vir} = 3 \times 10^{12} h^{-1} M_\odot$		$M_{vir} = 5 \times 10^{14} h^{-1} M_\odot$	
Moment	δ_l	δ	δ_l	δ	δ_l	δ
FSC	1.660	1203	1.652	770	1.631	377
VIR1	1.602	180	1.602	180	1.601	180
VIR2	1.628	340	1.629	340	1.628	340
COL	1.695	986	1.695	653	1.694	335

$\Omega_m = 0.3$, $\Omega_\Lambda = 0.7$

	$M_{vir} = 6.5 \times 10^{10} h^{-1} M_\odot$		$M_{vir} = 3 \times 10^{12} h^{-1} M_\odot$		$M_{vir} = 5 \times 10^{14} h^{-1} M_\odot$	
Moment	δ_l	δ	δ_l	δ	δ_l	δ
FSC	1.663	1170	1.655	761	1.637	392
VIR1	1.606	180	1.606	180	1.606	180
VIR2	1.632	340	1.632	340	1.632	340
COL	1.697	978	1.698	632	1.698	338

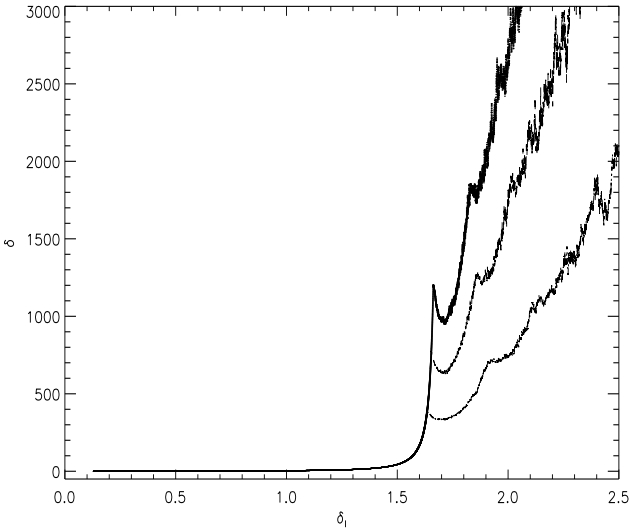

Figure 2. The relation $\delta_l - \delta$ for three virial masses. From down to top, the curves correspond to $M_{vir} = 5 \times 10^{14} h^{-1} M_\odot$, $M_{vir} = 3 \times 10^{12} h^{-1} M_\odot$ and $M_{vir} = 6.5 \times 10^{10} h^{-1} M_\odot$ (an Einstein-deSitter universe and M_{frac}=0.5 was used in all the cases).

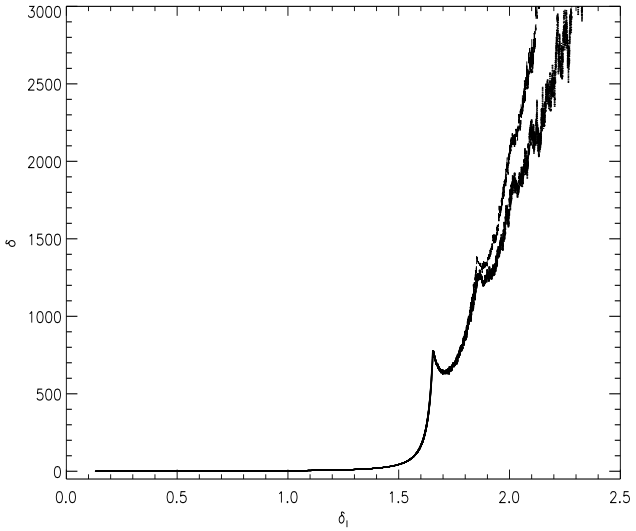

Figure 3. The relation $\delta_l - \delta$ for two different cosmologies. From down to top, the curves correspond to the Einstein-deSitter case and to the $\Omega_m = 0.3$, $\Omega_\Lambda = 0.7$ cosmology (a virial mass of $M_{vir} = 3 \times 10^{12} h^{-1} M_\odot$ and M_{frac}=0.5 was used in all the cases).

widely used in the entire literature, the reasons to make the assumptions given above lack a solid theoretical base (see section 3). In fact, there are some works that point to another direction and estimate other values of $\delta_{l,vir}$ and δ_{vir}. Jenkins et al. (2001), for example, find a better agreement with the simulations if δ_{vir} is taken constant for all the cosmologies and near the value that it takes in the Einstein deSitter cosmology ($\delta_{vir} \sim 180$). Also Avila-Reese, Firmani & Hernández (1998) find that a different value of $\delta_{l,vir}$ with respect to those obtained using the above assumptions makes better the comparison between the analytical Press-Schechter mass distribution and the results of N-body simulations.

Moreover, there is another important question related to the virialization that should be considered here. In the framework of the standard *SIM*, it is possible to apply the virial theorem if we suppose the halo to be an isolated system. However, real halos are non-isolated systems, with surrounding material continuously falling or escaping from the system. Hence, the virial theorem at least in the standard form could not be applied in this case. Despite of this fact, the standard *SIM* together with the virial theorem have

been used to obtain the values of $\delta_{l,vir}$ and δ_{vir}, and these values have been taken as the references to define the virial radius and the virial mass of the halos, which is specially adopted in N-body simulations. Furthermore, this fact has been traditionally supported for radial velocity early studies of massive dark matter halos from simulations (Crone et al. 1994; Cole & Lacey 1996). These studies apparently showed that the virial radius in this way defined (using $\delta_{l,vir} = 1.69$ and $\delta_{vir} \sim 180$ in the Einstein-deSitter) constitutes an adequate boundary to separate the inner region of the halo in dynamical equilibrium, i.e. that region where the radial velocities are zero, from the external region showing infall velocities. The popularization of these ideas came contemporaneously with works that defined the virial mass and virial radius in simulations according to these preliminary results (specially since the NFW papers). But the fact is that, as recently shown in Prada et al. (2006), this may not be totally correct. Concerning to galaxy-size halos, for example, they display all the properties of relaxed objects up to ~ 3 virial radius and there is no indication of infall of material beyond. Therefore, there is no reason to believe that only inside the virial radius, as currently defined, the halo is in equilibrium. In this context, it is important to understand the process of virialization more in depth.

In our work, no assumption is done related to the virialization. No collapse factor, no time for virialization *a priori* is adopted. Including shell-crossing in the way we do will allow us to obtain $\delta_{l,vir}$ and its corresponding δ_{vir} in a natural way, i.e. studying the evolution of different shells of the halo according to the *SST* framework, presented in section 2. It must be noted, however, that these values are still preliminary, since it will be necessary to include the effects of angular momentum, velocity dispersion and triaxiality to obtain precise and useful values. Nevertheless, this study will be suitable to isolate the role of shell-crossing and will be able to extract important conclusions related to the stabilization and virialization. We believe that these conclusions will not change when we introduce other physical considerations into the framework.

It is important to note here the difference between these two concepts: stabilization and virialization. The first one can be inferred studying the behaviour of the radius of a given shell that contains a given fraction of the virial mass with time, as was shown in Figure 1. A criterion must be imposed to say if a given shell reaches stabilization or not, and when. The second concept, the virialization, will have to be inferred according to the virial theorem. There is no reason why stabilization and virialization should coincide, although instinctively one expect that they should be near in time at least.

4.1 Stabilization

In first place, we define the time of stabilization as the time at which the radius of the shell that we are studying varies less than a given percent, and during -at least- an interval of time equal to once the time of turnaround. In practice, what we do is to choose the moment immediately after the time of first shell-crossing, and we see if there is no a variation in radius larger than the maximum variation that we want to impose as our criterion. It must be in this way during, at least, a time of turnaround from this moment onward. The value of reference that we take to measure the variations in radius is the value of the radius at the initial moment of this interval. If the stated percentage of variation of the radius is exceeded in any time within this interval, then we move ahead in time until we find an interval of time where the criterion is satisfied. The first moment at which this occurs is our time of stabilization, and the value of the radius at the time of stabilization is taken as our radius of stabilization.

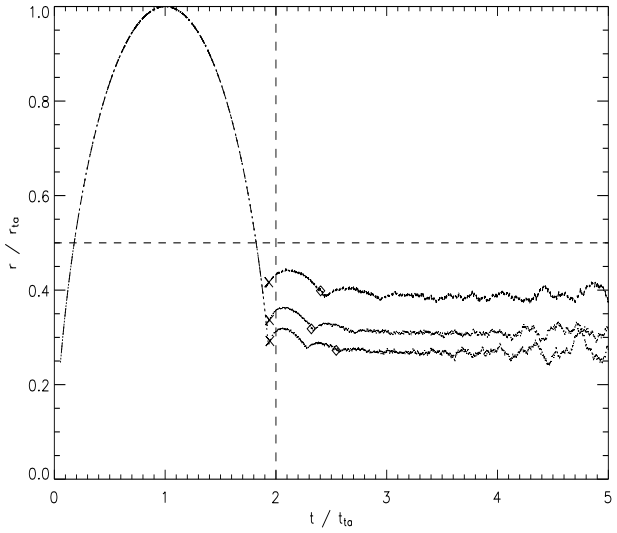

Figure 4. Stabilization at 5% (circles) and 10% (crosses) for a particular cosmology ($\Omega_m = 0.3$, $\Omega_\Lambda = 0.7$ and $M_{frac} = 0.5$ for three different virial masses. From down to top, the curves correspond to $M_{vir} = 6.5 \times 10^{10} h^{-1} M_\odot$ $M_{vir} = 3 \times 10^{12} h^{-1} M_\odot$ $M_{vir} = 5 \times 10^{14} h^{-1} M_\odot$. Again, the horizontal dashed-line corresponds to half the turnaround radius, and the vertical one the time of collapse, i.e. twice the turnaround time.

This is illustrated in Figure 4, where the moments of stabilization are shown for a 5% and 10% of allowed variation of radius, for a particular cosmology ($\Omega_m = 0.3$, $\Omega_\Lambda = 0.7$), a value of M_{frac}, and for different virial masses. As one can see, in the case of 10% the stabilization is reached inmediately after the first shell-crossing, but the stabilization according to only 5% of allowed variation of the radius is not reached until roughly half of a time unit later (in units of the turnaround time). Moreover, this stabilization remains during more than once the time of turnaround from that moment onward (which is the minimum required by our criterion). Only at late times, where the evolution is dominated by numerical noise, the stabilization becomes worse than 5%. However, the most important conclusion is that the stabilization is not reached in any case for a radius that is 1/2 the radius of turnaround, i.e. the value that corresponds to the collapse factor assumed in the standard derivation of $\delta_{l,vir}$ and δ_{vir}. This fact constitutes another proof that tell us how inappropriate are the current assumptions done about the virialization.

A detailed study was done for different values of M_{vir}, M_{frac} and different cosmologies. A summary of this study can be found in Appendix B, Tables B1 and B2. In these tables we present the values for the density contrasts that we obtain for two different degrees of stabilization (5% and

10%), varying M_{vir}, M_{frac} and for the Einstein-deSitter and $\Omega_m = 0.3$, $\Omega_\Lambda = 0.7$ cosmologies.

4.2 Virialization

Concerning to the virialization, what we did was to calculate the kinetic and potential energies related to the shell that we want to study. Then, we estimate the degree of agreement with respect to that given by the virial theorem (i.e. $U + 2K = 0$, where U and K are the potential and kinetic energies related to the shell under study) by means of the quantity:

$$VIR = \frac{|2K - U|}{2K} \tag{26}$$

It must be noted that, if the virial theorem was exactly satisfied by the shell at some moment of its evolution, this quantity should be at that time equal to zero.

The algorithm to define the moment and radius of virialization is the same as already described for the stabilization. When we find an interval where the degree of virialization that we want to impose is satisfied in every moment inside this interval, then we define our time and radius of virialization as those ones corresponding to the beginning of the interval considered. Again, as in the case of the stabilization, a detailed study was done for different values of M_{vir}, M_{frac} and different cosmologies. We summarize the results found in Tables B3 and B4 of Appendix B. In these tables we present the values for the density contrasts that we obtain for two different degrees of virialization (25% and 35%).

There is one issue related to Tables B3 and B4 that it is worth to mention. In those tables, a percent of 25% and 35% was set to look for virialization. This was done in this way because we noticed that below these percents it is impossible to reach virialization in most cases according to our criterion. A smaller percent means a degree of virialization too strong to be satisfied. Nevertheless, it seems that, when the virialization is reached using these high percents, the halo has *actually* reached the virialization. This may be inferred from the fact that the individual percents that we measure in every moment within the interval considered does not decrease monotonically from the beginning of the interval to its end. In fact, what one obtains is a small fluctuation around (and near) the high percent that was imposed to find the virialization. That is, the degree of virialization does not vary substantially within the whole interval, only small fluctuations are found. There is a possible explanation to the fact that we have actually reached virialization but the degree of virialization that we find according to our definition is still above 20% or more. Until now, we have used the standard virial theorem, that only involves the kinetic and potential energies. However, because of the fact that we are treating with a non-isolated system, with shells of matter continuously going in and going out from the system that we are considering as our halo, we should include in the theorem another extra term. This term would be related to the pressures involved in the system, and surely may be the explanation and the cause of this "residual" percent that we obtain in all the cases.

4.3 Comparison between stabilization and virialization: general considerations

A summary of our results concerning to the degree of both stabilization and virialization for a given shell can be found in Tables 4 and 5. In these tables, we show the degree of stabilization (STA) and virialization (VIR) reached for two known moments of evolution, $VIR1$ and $VIR2$ (see section 3), for different values of M_{vir}, M_{frac} and different cosmologies. The degree of virialization, *VIR*, is calculated using Eq.(26) for moments $VIR1$ and $VIR2$. Concerning to the degree of stabilization, it was estimated by calculating the following factor:

$$STA = \frac{r_{VIR} - r_{STA}}{r_{STA}} \tag{27}$$

where r_{VIR} is the value of the radius when $\delta = 180$ (VIR1) or when $\delta = 340$ (VIR2), and r_{STA} is the value of the radius at the moment of stabilization, this one calculated according to the method described in section 4.1 and using a value of 10% for the allowed variation in radius. This factor *STA* can be understood as a factor that measures the relative contraction of the radius at times *VIR1* or *VIR2* with respect to that found at the moment of stabilization.

Both tables provide useful results to extract important conclusions. In first place, one can see that the points $VIR1$ and $VIR2$ are really far from the stabilization and also from the virialization, although these points are the preferred values for the moment of virialization in most of the works found in the literature. In fact, in all the cases the first shell-crossing occurs even after $VIR1$ and $VIR2$, as pointed in section 3, so it is not possible that the shell has reached virial equilibrium or simply stabilization in radius at that moment. Also Lemson (1995) found similar results using N-body simulations, i.e. the equilibrium is reached in a longer time respect to that predicted by the standard *SIM*. In most of the cases, both stabilization and virialization were obtained far from the value $\delta_l = 1.686$ or $\delta_l = 1.676$, the preferred values of $\delta_{l,vir}$ for the Einstein-deSitter and the $\Omega_m = 0.3$, $\Omega_\Lambda = 0.7$ cosmology respectively (see Appendix B, Tables B1 to B4). Concerning to the associated values of the actual density contrast, δ, we find very high values in most cases. It should be noted, however, that it is expected that these values decrease substantially when we include angular momentum and velocity dispersion in the formalism. So, the values showed in these tables are totally related to the isolated effect of shell-crossing.

There are also other issues that could be interesting to stress, and that should be explored in more detail in a future work:

(i) Concerning to $VIR1$ and $VIR2$, the degree of both virialization and stabilization are better for larger values of M_{vir}.

(ii) Concerning to $VIR1$ and $VIR2$, the degree of both virialization and stabilization are also better for larger values of M_{frac}.

(iii) Concerning to $VIR1$ and $VIR2$, the degree of both virialization and stabilization are worse in the $\Omega_m = 0.3$, $\Omega_\Lambda = 0.7$ cosmology.

(iv) The moment of stabilization is reached earlier in the $\Omega_m = 0.3$, $\Omega_\Lambda = 0.7$ cosmology.

Table 4. Degree of agreement with the virial theorem (VIR) and stabilization (STA), calculated according to equations (26) and (27), for two moments of evolution VIR1 and VIR2, and for different values of M_{frac} and two cosmologies. A virial mass of $M_{vir} = 3\times10^{12}h^{-1}M_{\odot}$ was used in all the cases.

Einstein-deSitter ($\Omega_m = 1$, $\Omega_\Lambda = 0$)

	$M_{frac}=0.2$		$M_{frac}=0.5$		$M_{frac}=0.8$		$M_{frac}=1.0$		$M_{frac}=1.3$	
Moment	VIR	STA	VIR	STA	VIR	STA	VIR	STA	VIR	STA
VIR1	4.64	0.57	2.98	0.43	2.58	0.33	1.01	0.25	1.04	0.19
VIR2	4.12	0.47	2.80	0.31	1.01	0.19	1.01	0.09	0.36	0.09

$\Omega_m = 0.3$, $\Omega_\Lambda = 0.7$

	$M_{frac}=0.2$		$M_{frac}=0.5$		$M_{frac}=0.8$		$M_{frac}=1.0$		$M_{frac}=1.3$	
Moment	VIR	STA	VIR	STA	VIR	STA	VIR	STA	VIR	STA
VIR1	4.32	0.49	2.75	0.35	1.80	0.23	1.42	0.19	1.06	0.13
VIR2	3.88	0.39	2.40	0.21	1.65	0.07	1.31	0.05	0.98	0.07

(v) The moment of virialization is reached earlier for smaller values of M_{vir}.

(vi) The moment of virialization is reached earlier for larger values of M_{frac}. It is worth to mention that Lemson (1995) found the same from his simulations, i.e. the inner shells reach equilibrium later.

(vii) The moment of virialization is reached later in the $\Omega_m = 0.3$, $\Omega_\Lambda = 0.7$ cosmology.

(viii) It seems that there is no coincidence in time between virialization and stabilization, although it should substantially depend on the percent that we impose to define both concepts.

(ix) For all values of M_{frac} and M_{vir}, the stabilization in radius occurs at a fraction of the turnaround radius that is different from that given by the collapse factor (1/2 in the Einstein-deSitter case). The same is valid for the $\Omega_m = 0.3$, $\Omega_\Lambda = 0.7$ cosmology.

5 SUMMARY AND FUTURE WORK

In this work we have studied the effect of shell-crossing in the formation and subsequent evolution of dark matter halos. To do that, we have used the spherical collapse model, which has been widely used in the literature for more than thirty years to manage and solve questions related to these processes. Despite of the large amount of works that have used this model or many others that have improved it by introducing in the formalism more and more complex considerations, only a few of them have included the effect of shell-crossing. Moreover, most of these works have managed this effect analytically using the adiabatic invariant as a good approximation.

Here we handle the effect of shell-crossing numerically. This allows us to study individually any shell of matter involved in the process of formation of the halo. Doing so, we can extract multiple conclusions about the way in which this process occurs, like the relation between the linear and actual density contrasts, the process of stabilization of a shell of matter, the virialization, etc. Most of these issues have been treated in the present work to a greater or lesser extent, although the main goal have always been the developing of an adequate framework - named as Spherical Shell Tracker (SST) - in which we can study in depth the shell crossing and also other secondary effects.

It is possible to summarize the main conclusions of this work as follows:

(i) The *SST* framework is adequate to tackle the effect of shell-crossing in a way that allow us to extract exact results for different issues related to the evolution of the halo: the way that the radius of a given shell evolves with time, the relation between the linear and actual density contrasts, the stabilization, the virialization, etc.

(ii) The shell-crossing by itself is able to produce stabilization and virialization. Nevertheless, for the moment, it is not possible to obtain the exact values of the linear and actual density contrasts related to both moments of evolution. It is necessary to take into account also other important effects, such as angular momentum, velocity dispersions or triaxiality.

(iii) Concerning to the relation between the linear and actual density contrasts, the dependence of this relation with the cosmology is very small and practically negligible. This conclusion is contrary to most of previous works, which find in general a large dependence with cosmology. However, the dependence with the virial mass or the fraction of virial mass that we consider, is large.

(iv) Neither stabilization nor virialization are reached in a time according to that given by the common assumptions related to the collapse factor and the time of virialization. In all the cases, we find that both stabilization and virialization occur at later times.

(v) The values typically used in the literature for $\delta_{l,vir}$ and δ_{vir} seem to be clearly inadequate and incorrect, and are based on not very solid assumptions. In this work, new values of $\delta_{l,vir}$ and δ_{vir} are presented, but only taking into account the effect of shell-crossing. It will be necessary to include in our framework other effects also relevant to be able to provide useful and final values for $\delta_{l,vir}$ and δ_{vir}.

It is worth to emphasize that this work constitutes only a first step in our attempt to obtain exact and precise pre-

Table 5. Degree of agreement with the virial theorem (VIR) and stabilization (STA), calculated according to equations (26) and (27), for two moments of evolution VIR1 and VIR2, and for three different virial masses and two cosmologies. A value of $M_{frac} = 0.5$ was used in all the cases. See text for details.

Einstein-deSitter ($\Omega_m = 1$, $\Omega_\Lambda = 0$)

	$M_{vir} = 6.5 \times 10^{10} h^{-1} M_\odot$		$M_{vir} = 3 \times 10^{12} h^{-1} M_\odot$		$M_{vir} = 5 \times 10^{14} h^{-1} M_\odot$	
Moment	VIR	STA	VIR	STA	VIR	STA
VIR1	2.62	0.51	2.98	0.43	2.14	0.23
VIR2	2.36	0.41	2.80	0.31	2.21	0.05

$\Omega_m = 0.3$, $\Omega_\Lambda = 0.7$

	$M_{vir} = 6.5 \times 10^{10} h^{-1} M_\odot$		$M_{vir} = 3 \times 10^{12} h^{-1} M_\odot$		$M_{vir} = 5 \times 10^{14} h^{-1} M_\odot$	
Moment	VIR	STA	VIR	STA	VIR	STA
VIR1	3.50	0.43	2.75	0.35	1.18	0.17
VIR2	2.86	0.31	2.40	0.21	1.14	0.05

dictions related to the formation and evolution of dark matter halos. In a future work we plan to include in the *SST* framework other important effects that it will be absolutely necessary. In particular, including the angular momentum and velocity dispersion will be the next step. Furthermore, in parallel, we will implement a more sophisticated initial density profile than that used in this work, which fits better that found in the simulations and could change the results presented here only slightly. It is also in our mind to use cosmological N-body simulations, since comparison between both analytical and simulation studies will be, by sure, crucial to reach a better and deeper understanding of the processes involved in the formation and evolution of dark matter halos.

ACKNOWLEDGMENTS

We thank to J.A. Rubiño-Martín for useful comments and discussions. M.A.S.C. acknowledges the support of an I3P-CSIC fellowship in Granada. M.A.S.C., J.B.R. and F.P. also thank the support of the Spanish AYA2005-07789 grant.

APPENDIX A: THE FORMALISM IN THE ΛCDM COSMOLOGY

If we are in a $\Lambda \neq 0$ cosmology, we need to introduce some changes for the initial conditions and in the expressions for the evolution of the spherical perturbation, although the formalism and the algorithm are essentially the same as presented in section 2, i.e. the *SST* framework.

The equation for the initial radii of the shells is the same as given by Eq.(18), but for the velocities the correct expression, instead of Eq.(19), is now:

$$v_i(j) = \left[1 - \frac{1}{3} \frac{1}{1+\delta(\delta_l^i(q(j)))} \frac{a_i\ \dot{D}(a)}{D(a)} \Big|_{a=a_i} \frac{\delta_l^i(q(j))}{\frac{d\delta_l(\delta)}{d\delta}\big|_{\delta=\delta(\delta_l^i(q(j)))}} \right] \times\ r_i(j)\ \frac{2}{3}\ (1+\beta_i)^{\frac{1}{2}}\ ln\left[\beta_i^{-\frac{1}{2}} + \sqrt{1+\beta_i^{-1}} \right] \quad \text{(A1)}$$

where

$$\dot{D}(a) = \frac{dD(a)}{da}$$

$$\beta_i = \frac{\Omega_m}{\Omega_\Lambda}\ (1+z_i)^3 = \beta_0\ (1+z_i)^3$$

and,

$$a(t) = \left[\beta_0^{\frac{1}{2}} \left(\frac{(\beta_i^{-\frac{1}{2}} + \sqrt{1+\beta_i^{-1}})^t - (\beta_i^{-\frac{1}{2}} + \sqrt{1+\beta_i^{-1}})^{-t}}{2} \right) \right]^{\frac{2}{3}}$$

$$a_i = \frac{1}{1+z_i}$$

$$D(a) = \frac{1}{2\ a\ f(a)} \int_0^a f^3(a)\ da$$

$$f(a) = \left[1 + \Omega_m \left(\frac{1}{a} - 1 \right) + \Omega_\Lambda (a^2 - 1) \right]^{-\frac{1}{2}} \quad \text{(A2)}$$

Note that β_i is simply the parameter $\beta_0 = \Omega_m/\Omega_\Lambda$ but referred to the initial time.

Concerning to the initial density profile, now the initial linear density contrast is essentially the same as given by Eq.(15) but now the rescaling factor, $\frac{1}{1+z_i}$, is here replaced by $\frac{D(a_i)}{D(a=1)}$, which gives:

$$\delta_l^i(q(j)) = \frac{D(a_i)}{D(a=1)}\ \delta_l(q(j)) \quad \text{(A3)}$$

where $\delta_l(q(j))$ is the linear profile given by Eq.(12).

For the evolution, equations (21) and (22) are still valid for the radius and the velocity, but to compute the linear and actual density contrast, now we have to include:

$$\delta_l(j,t) = \frac{D(a(t))}{D(a_i)}\ \delta_l^i(q(j)) \quad \text{(A4)}$$

$$\delta(j,t) = \left[[1+\delta(\delta_l^i(q(j)))] \left(\frac{r_i(j)}{r(j)} \right)^3 \left(\frac{a(t)}{a_i} \right)^3 \right] - 1 \quad \text{(A5)}$$

where $D(a)$ and $a(t)$ are the growing and scale factor respectively, as defined in Eq.(A2), and a_i denotes the scale factor at initial time, given also in Eq.(A2).

To recompute the enclosed mass at each time step, it is also necessary to take into account the new cosmology, once we have calculated $M(j,t)$ in first place according to Eq.(25), i.e.:

$$M(j,t)(\Lambda \neq 0) = M(j,t)(\Lambda = 0) - \frac{2}{\beta_i} r(j,t)^3 \qquad \text{(A6)}$$

APPENDIX B: RESULTS OBTAINED FOR STABILIZATION AND VIRIALIZATION

In Tables B1 to B4 the linear and actual density contrasts that we obtain concerning to the moments of stabilization and virialization are shown. Tables B1 and B2 refer to the stabilization, whereas Tables B3 and B4 are related to the virialization. In both cases, the moments of stabilization and virialization were matched following the criteria given in Section 4. In these Tables, linear and actual density contrast are shown for different values of virial mass, M_{vir}, fraction of virial mass, M_{frac}, and for Einstein-deSitter and $\Omega_m = 0.3$, $\Omega_\Lambda = 0.7$ cosmologies.

REFERENCES

Avila-Reese, V., Firmani, C. & Hernandez, X. 1998, ApJ, 505, 37

Ascasibar, Y., Yepes, G., Gottloeber, S. & Mueller, V. 2004, MNRAS, 352, 1109

Bardeen, J. M., Bond, J. R., Kaiser, N. & Szalay, A. S. 1986, ApJ, 304, 15 (BBKS)

Barkana R., 2004, MNRAS, 347, 59

Bertschinger, E. 1985, ApJS, 58,39

Betancort-Rijo J., Sánchez-Conde M.A., Prada F., Patiri S.G., 2006, ApJ, in press, astro-ph/0509897

Bondi H., 1947, MNRAS, 107, 410

Bryan G., Norman M., 1998, ApJ, 495, 80

Cole S., Lacey C., 1996, MNRAS, 281, 716

Crone M.M., Evrard A.E., Richstone D.O., 1994, ApJ, 432, 402

Dubinski J., Carlsberg R.G., 1991, ApJ, 378, 496

Eke V.R., Cole S., Frenk C.S., 1996, MNRAS, 282, 263

Fillmore, J. A. & Goldreich, P. 1984, ApJ, 281, 1

Frenk C.S., White S.D.M., Davis M., Efstathiou G., 1988, ApJ, 327, 507

Gunn, J. E. & Gott, J. R. 1972, ApJ, 176, 1

Gunn J. E., 1977, ApJ, 218, 592

Hiotelis, N. 2002, å, 382, 84

Hoffman Y., Shaham J., 1985, ApJ, 297, 16

Jenkins A., Frenk C. S., White S. D. M., Colberg J. M., Cole S., Evrard A. E., Couchman H. M. P., Yoshida N., 2001, MNRAS, 321, 372

Jing Y.P., Suto Y., 2000, ApJ, 529, L69

Klypin A., Kravtsov A.V., Bullock J.S., Primack J.R., 2001, ApJ, 554, 903

Lacey C., Cole S., 1994, MNRAS, 271, 676

Lahav O., Lilje P.B., Primack J.R., Rees M.J., 1991, MNRAS, 251, 128

Lemson G., 1995, PhD: Statistics and dynamics of the perturbed universe, Groningen University

Lokas E. L., 2000, MNRAS, 311, 423

Lokas, E. L. & Hoffman, Y. 2000, ApJ, 542, L139

Lu Y., Mo H.J., Katz N., Weinberg D., 2006, MNRAS, 368, 1931

Manrique A., Raig A., Salvador-Solé E., Sanchis T., Solanes J.M., 2003, ApJ, 593, 26

Martnez V.J., Saar E., 2002, Statistics of galaxy distribution, Chapman & Hall/CRC

Moore B., Governato F., Quinn T., Stadel J., Lake G., 1998, ApJ, 499, L5

Moore B., Quinn T., Governato F., Stadel J., Lake G., 1999, MNRAS, 310, 1147

Navarro, J.F., Frenk C.S., White S.D.M., 1996, ApJ, 462, 563

Navarro, J.F., Frenk C.S., White S.D.M., 1997, ApJ, 490, 493

Nusser A., Sheth R.K., 1999, MNRAS, 303, 685

Nusser, A. 2001, MNRAS, 325, 1397

Padmanabhan T., 1993, Structure formation in the Universe, Cambridge University Press, Cambridge

Padmanabhan T., 1996, MNRAS, 278, L29

Patiri S., Betancort-Rijo J. E. & Prada F., 2004, MNRAS, 368, 1132

Peebles P.J.E., 1980, The large-scale structure of the universe, Princeton University Press, Princeton, N.J.

Prada F., Klypin A. A., Simmoneau E., Betancort-Rijo J., Patiri S. G., Gottlöber S., Sánchez-Conde M. A., 2006 ApJ, 645, 1001

Press W.H., Schechter P., 1974, ApJ, 187, 425

Ricotti M., 2003, MNRAS, 344, 1237

Quinn P.J., Salmon J.K., Zurek W.H., 1986, Nat, 322, 329

Shapiro P.R., Illiev I.T., Martel H., Alvarez M.A., 2004, astro-ph/0409173

Sheth, R. K. & Tormen, G. 2002, MNRAS, 329, 61

Subramanian K., Cen R., Ostriker J. P., 2000, ApJ, 538, 528

Tolman R.C., 1934, Relativity, Thermodynamics, and Cosmology. Clarendon Press, Oxford

Table B1. Linear and actual density contrasts at the moment of stabilization, this one defined according to two percentages (5% and 10%), for different values of M_{frac} and two cosmologies. A virial mass of $M_{vir} = 3 \times 10^{12} h^{-1} M_{\odot}$ was used in all the cases. See text for details.

Einstein-deSitter ($\Omega_m = 1$, $\Omega_\Lambda = 0$)

	$M_{frac} = 0.2$		$M_{frac} = 0.5$		$M_{frac} = 0.8$		$M_{frac} = 1.0$		$M_{frac} = 1.3$	
Percentage	δ_l	δ	δ_l	δ	δ_l	δ	δ_l	δ	δ_l	δ
5 %	-	-	-	-	-	-	-	-	-	-
10 %	1.98	3993	2.00	1789	2.05	1223	1.89	700	1.90	537

$\Omega_m = 0.3$, $\Omega_\Lambda = 0.7$

	$M_{frac} = 0.2$		$M_{frac} = 0.5$		$M_{frac} = 0.8$		$M_{frac} = 1.0$		$M_{frac} = 1.3$	
Percentage	δ_l	δ	δ_l	δ	δ_l	δ	δ_l	δ	δ_l	δ
5 %	1.91	3306	1.85	1298	1.86	897	1.86	741	1.86	621
10 %	1.67	1496	1.67	703	1.67	463	1.67	390	1.67	324

Table B2. Linear and actual density contrasts at the moment of stabilization, this one defined according to two percentages (5% and 10%), for three different virial masses and two cosmologies. A value of $M_{frac} = 0.5$ was used in all the cases. See text for details.

Einstein-deSitter ($\Omega_m = 1$, $\Omega_\Lambda = 0$)

	$M_{vir} = 6.5 \times 10^{10} h^{-1} M_{\odot}$		$M_{vir} = 3 \times 10^{12} h^{-1} M_{\odot}$		$M_{vir} = 5 \times 10^{14} h^{-1} M_{\odot}$	
Percentage	δ_l	δ	δ_l	δ	δ_l	δ
5 %	-	-	-	-	-	-
10 %	-	-	2.00	1789	1.87	610

$\Omega_m = 0.3$, $\Omega_\Lambda = 0.7$

	$M_{vir} = 6.5 \times 10^{10} h^{-1} M_{\odot}$		$M_{vir} = 3 \times 10^{12} h^{-1} M_{\odot}$		$M_{vir} = 5 \times 10^{14} h^{-1} M_{\odot}$	
Percentage	δ_l	δ	δ_l	δ	δ_l	δ
5 %	1.93	2727	1.85	1298	1.89	680
10 %	1.67	1105	1.67	703	1.67	352

Table B3. Linear and actual density contrasts at the moment of virialization, this one defined according to two percentages (25% and 35%), for different values of M_{frac} and two cosmologies. A virial mass of $M_{vir} = 3 \times 10^{12} h^{-1} M_{\odot}$ was used in all the cases. See text for details.

Einstein-deSitter ($\Omega_m = 1$, $\Omega_\Lambda = 0$)

	$M_{frac} = 0.2$		$M_{frac} = 0.5$		$M_{frac} = 0.8$		$M_{frac} = 1.0$		$M_{frac} = 1.3$	
Percentage	δ_l	δ	δ_l	δ	δ_l	δ	δ_l	δ	δ_l	δ
25 %	2.25	6843	2.09	2080	1.97	903	1.90	731	1.81	347
35 %	2.25	6843	2.09	2080	1.97	903	1.90	731	1.81	347

$\Omega_m = 0.3$, $\Omega_\Lambda = 0.7$

	$M_{frac} = 0.2$		$M_{frac} = 0.5$		$M_{frac} = 0.8$		$M_{frac} = 1.0$		$M_{frac} = 1.3$	
Percentage	δ_l	δ	δ_l	δ	δ_l	δ	δ_l	δ	δ_l	δ
25 %	-	-	-	-	-	-	-	-	2.20	2495
35 %	2.43	13277	2.26	4374	2.13	2070	2.06	1574	1.96	879

Table B4. Linear and actual density contrasts at the moment of virialization, this one defined according to two percentages (25% and 35%), for three different virial masses and two cosmologies. A value of $M_{frac} = 0.5$ was used in all the cases. See text for details.

Einstein-deSitter ($\Omega_m = 1$, $\Omega_\Lambda = 0$)

	$M_{vir} = 6.5 \times 10^{10} h^{-1} M_\odot$		$M_{vir} = 3 \times 10^{12} h^{-1} M_\odot$		$M_{vir} = 5 \times 10^{14} h^{-1} M_\odot$	
Percentage	δ_l	δ	δ_l	δ	δ_l	δ
25 %	1.89	1971	2.09	2080	- [1]	- [1]
35 %	1.89	1971	2.09	2080	- [1]	- [1]

[1] In this case, no virialization was obtained below 45%; for this percentage, $\delta_l = 2.32$ and $\delta = 1429$

$\Omega_m = 0.3$, $\Omega_\Lambda = 0.7$

	$M_{vir} = 6.5 \times 10^{10} h^{-1} M_\odot$		$M_{vir} = 3 \times 10^{12} h^{-1} M_\odot$		$M_{vir} = 5 \times 10^{14} h^{-1} M_\odot$	
Percentage	δ_l	δ	δ_l	δ	δ_l	δ
25 %	2.11	4387	-	-	2.43	3092
35 %	2.03	3509	2.26	4374	2.31	2111